# 1Gbps free-space deep-ultraviolet communications based on III-nitride micro-LEDs emitting at 262nm

# 1 Gbps free-space deep ultraviolet communications based on III-nitride micro-LEDs emitting at 262 nm

XIANGYU HE[1,*], ENYUAN XIE[1,*,#], MOHAMED SUFYAN ISLIM[2,*], ARDIMAS ANDI PURWITA[2], JONATHAN J. D. MCKENDRY[1], ERDAN GU[1,#], HARALD HAAS[2], AND MARTIN D. DAWSON[1]

[1] Institute of Photonics, Department of Physics, University of Strathclyde, Glasgow, G1 1RD, UK
[2] Li–Fi R&D Centre, the University of Edinburgh, Institute for Digital Communications, King's Buildings, Mayfield Road, Edinburgh EH9 3JL, UK
[*] These authors contributed equally to this work
[#] Corresponding authors: enyuan.xie@strath.ac.uk, erdan.gu@strath.ac.uk

Compiled March 27, 2019

**The low modulation bandwidth of deep ultraviolet (UV) light sources is considered as the main reason limiting the data transmission rate of deep UV communications. Here, we present high-bandwidth III-nitride micro-light emitting diodes ($\mu$LEDs) emitting in the UV-C region and their applications in deep UV communication systems. The fabricated UV-C µLEDs with 566 $\mu m^2$ emission area produce an optical power of 196 $\mu$W at the 3400 A/cm$^2$ current density. The measured 3-dB modulation bandwidth of these $\mu$LEDs initially increases linearly with the driving current density and then saturates as 438 MHz at a current density of 71 A/cm$^2$, which is limited by the cut-off frequency of the commercial avalanche photodiode used for the measurement. A deep UV communication system is further demonstrated. By using the UV-C $\mu$LED, up to 800 Mbps and 1.1 Gbps data transmission rates at bit error ratio of 3.8 $\times$ $10^{-3}$ are achieved assuming on–off-keying and orthogonal frequency division multiplexing modulation schemes, respectively.** 

http://dx.doi.org/10.1364/ao.XX.XXXXXX

## 1. INTRODUCTION

Deep ultraviolet (UV) communications have gained great interest recently due to a number of advantages compared with visible light communications. It is well known that solar radiation has a strong influence on visible light based optical communication links due to the high background noise [1]. However, most of the solar UV radiation especially in the UV-C band between 200 nm and 280 nm is absorbed by the ozone layer in Earth's stratosphere. This results in the negligible deep UV radiation at ground level [2]. Therefore, the background noise is negligibly low for both indoor and outdoor deep UV optical wireless communications [3]. Meanwhile, due to the strong scattering of deep UV light in the air [4], a non-line-of-sight (NLOS) communication link, which has reduced pointing, acquisition and tracking requirements, can be constructed by using deep UV light sources [5]. Furthermore, due to the strong UV absorption by the ozone layer as mentioned, deep UV communication links between satellites would be hardly traceable at ground level. Therefore, outer space deep UV communications are highly secure. Recently, many research efforts concentrated on deep UV communications motivated by the fast development of deep UV light sources, filters [6] and detectors [6, 7]. However, the reported data transmission rates of the deep UV communications are still quite low [6–9] and, to the best of our knowledge, the reported highest data transmission rate at bit error ratio (BER) of 3.8 $\times$ $10^{-3}$ so far is 71 Mbps [10]. This is mainly caused by the low modulation bandwidth of the deep UV light sources used in the systems. In the early works, deep UV flash tubes or lamps were used. These light sources have very low modulation bandwidths, typically less than 40 kHz [8]. Recently, semiconductor UV light emitting diodes (LEDs) have been used for deep UV communications [3, 10]. Compared with the UV flashtubes or lamps, the modulation bandwidth of UV LEDs is much higher. A deep UV LED with a modulation bandwidth of 153 MHz was reported recently [3]. However, conventional LEDs have a large chip size, typically in the millimeter range, which leads to a large resistance-capacitance (RC) time constant and, thus, limits the further increase in modulation bandwidth [11]. In order to achieve deep UV communications with much higher data transmission rates, it is of paramount importance to develop novel deep UV light sources with high modulation bandwidths.

Micro-LEDs ($\mu$LEDs), of edge dimension/diameter typically in the 10-100 $\mu$m range, have many inherent advantages for visible light communication applications [12]. Thanks to their small junction areas, $\mu$LEDs present a small capacitance [13]. Thus, compared with conventional broad-area LEDs, the modulation bandwidth of $\mu$LEDs is mainly dominated by differential carrier

lifetime rather than the RC time constant [14]. Furthermore, $\mu$LEDs can be driven at very high current densities, which leads to a short differential carrier lifetime and thus a high modulation bandwidth [13]. Therefore, $\mu$LEDs are highly suitable light sources for high-speed optical communications. In our recent work, an over 800 MHz 6-dB electrical modulation bandwidth was achieved for polar $\mu$LEDs [15]. Moreover, by using the non-polar $\mu$LED, an over 1 GHz 3-dB electrical modulation bandwidth has also been reported [16, 17]. By using a single visible $\mu$LED as a transmitter, a 7.91 Gbps data transmission rate was achieved at the BER of $3.8 \times 10^{-3}$ with orthogonal frequency division multiplexing (OFDM) modulation schemes [18]. However, to the best of our knowledge, deep UV $\mu$LEDs and their applications in the free-space optical communication have not yet been demonstrated.

In this paper, we present a III-nitride $\mu$LED device emitting at 262 nm and characterize its performance for the deep UV communications. At a current density of 3400 A/cm$^2$ in direct-current (DC) operation, the optical power of this deep UV $\mu$LED is over 190 $\mu$W, corresponding to an optical power density of 35 W/cm$^2$. The measured 3-dB electrical modulation bandwidth of this $\mu$LED is over 400 MHz at a driving current density of 71 A/cm$^2$, which is 3 times higher than the reported bandwidth of deep UV LEDs. By using this high-bandwidth $\mu$LED as a deep UV light source, a deep UV communication system is established. Up to 800 Mbps and 1.1 Gbps error-free data transmission rates at the BER of $3.8 \times 10^{-3}$ are achieved assuming on-off keying (OOK) and OFDM modulation schemes, respectively. To the best of our knowledge, these data transmission rates are more than 15 times higher than the reported results at the same BER value in the deep UV wavelength band [10], which demonstrates the great potential of $\mu$LEDs for the deep UV communications.

## 2. UV-C $\mu$LEDS

### A. Design and fabrication of the UV-C $\mu$LED array

A commercial AlGaN-based LED wafer grown on a c-plane sapphire substrate with a 262 nm emission wavelength was used in this work for the $\mu$LED fabrication. The epitaxial structure of this wafer includes a 2 $\mu$m-thick AlN buffer layer, a 2 $\mu$m-thick n-doped $Al_{0.6}Ga_{0.4}N$ layer, an active region consisting of 6-period AlGaN-based quantum wells (QWs) with the 2.5 nm-thick well and 13 nm-thick barrier, a 50 nm-thick $Al_{0.6}Ga_{0.4}N$ electron blocking layer (EBL) and finally a 310 nm-thick p-doped GaN layer. The Al compositions in the wells and barriers are estimated as 45% and 55%, respectively. The $\mu$LEDs were fabricated in a 'concentric cluster' array format. The design and fabrication process of the $\mu$LED array presented in this work were similar to those reported in our previous work [15, 18, 19]. This $\mu$LED array consists of 15 $\mu$LEDs in a flip-chip configuration, each of trapezoidal shape with an emission area of 566 $\mu$m$^2$. This area is equivalent to a disk shape $\mu$LED with a diameter of 27 $\mu$m. With a shared cathode, each $\mu$LED is individual addressed by its corresponding anode. Fig. 1 illustrates the cross-sectional schematic of a single UV-C $\mu$LED fabricated in this work. As shown, in order to reduce the capacitance and, thus, increase the modulation bandwidths of the $\mu$LEDs, the $\mu$LED structure was created by two $Cl_2$-based inductively coupled plasma (ICP) etching processes. Firstly, 15 $\mu$LEDs were defined by ICP etching which terminated at the n-type AlGaN layer. Then, an n-type AlGaN mesa was created by further ICP etching down to the sapphire substrate. An annealed Pd layer with a thickness of 100 nm was used as the quasi-ohmic p-type metal contact to p-type GaN [11]. A metal bilayer of Ti/Au (50 nm/300 nm) was used as the n-type contact and metal tracks to connect the $\mu$LEDs. Fig. 2(a) shows the optical images of the fabricated UV-C $\mu$LED array presented in this work. A high-magnification image of the $\mu$LEDs is shown in Fig. 2(b). During this work, all the measurements were performed on bare, unpackaged $\mu$LED die.

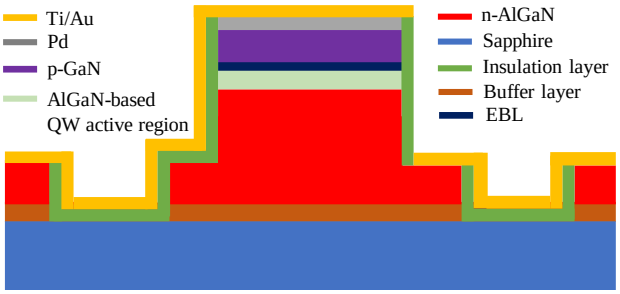


**Fig. 1.** Simplified cross-sectional schematic of a single UV-C $\mu$LED presented in this work. Dimensions are not to scale.

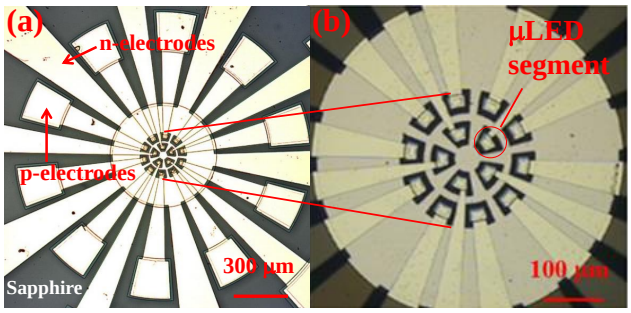


**Fig. 2.** (a) Plan view optical image of the fabricated UV-C $\mu$LED array presented in this work and (b) a high magnification image of the $\mu$LEDs.

### B. Electrical, optical and modulation bandwidth characteristics of the UV-C $\mu$LEDs

Fig. 3 presents the typical current density–voltage (*J-V*) and optical power-current density (*L-J*) curves of a single UV-C $\mu$LED from the fabricated $\mu$LED array. The inset in Fig. 3 presents the emission spectrum of the UV-C $\mu$LED at 1768 A/cm$^2$. The *J-V* and *L-J* data were measured at the same time by placing a UV enhanced Si photodetector in close proximity to the polished sapphire substrate of the $\mu$LED. The *J-V* curve shows that the turn-on voltage of this $\mu$LED is 13 V at 180 A/cm$^2$ (1mA). This value is consistent with that reported in previous work on broad-area UV-C LEDs [20]. For this UV-C $\mu$LED, such the high turn-on voltage is mainly attributed to the high contact resistivity of metal contact to n-type $Al_{0.6}Ga_{0.4}N$ layer. 60% Al composition in this n-type $Al_{0.6}Ga_{0.4}N$ results in the difficulty to achieve high-quality ohmic contact [21]. In order to reduce the turn-on voltage, we are currently working on optimising the metal contact to n-type $Al_{0.6}Ga_{0.4}N$ layer by testing different metal schemes and annealing processes. Furthermore, this $\mu$LED can be driven at a current density up to 3400 A/cm$^2$ before thermal rollover. This maximum current density is much higher than the current densities (125 A/cm$^2$) that the conventional deep UV LEDs can sustain [22]. At this current density, the unidirectional optical power output of the $\mu$LED is 196 $\mu$W at the sapphire

substrate surface, corresponding to an optical power density of 35 W/cm$^2$.

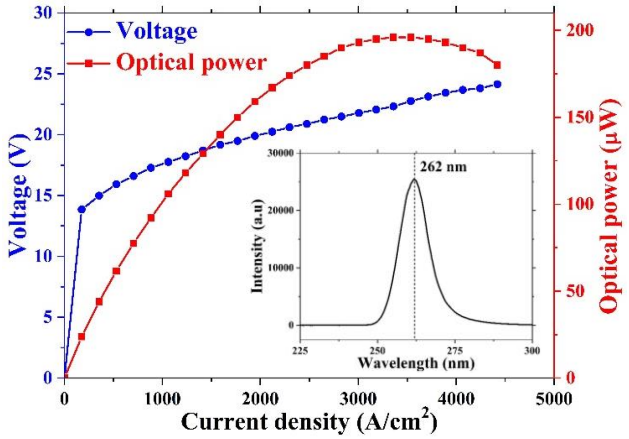


**Fig. 3.** *J-V* and *L-J* characteristics of a UV-C $\mu$LED. The inset shows the emission spectrum of a UV-C $\mu$LED at 1768 A/cm$^2$.

As mentioned above, the modulation bandwidth of $\mu$LEDs is mainly dominated by the differential carrier lifetime rather than the RC time constant. The differential carrier lifetime is reduced when the operating current density increases and, compared with conventional LEDs, operating current density of $\mu$LEDs is much higher. Therefore, a high modulation bandwidth is expected for the UV-C $\mu$LEDs fabricated in this work. To verify this, the frequency response of these UV-C $\mu$LEDs were measured following a similar method to that described in our previous work [18]. An alternating current frequency sweep signal from a network analyzer was combined with a DC-bias current in a bias-tee (SHF BT45-D), and then sent to modulate the $\mu$LED. The optical response from the $\mu$LED was firstly collected by two UV enhanced optical lenses and, then, focused by a UV enhanced objective lens into an UV enhanced Si avalanche photodiode (APD) detector (Thorlab APD430A2(/M)) with a specified output 3-dB electrical bandwidth between DC to 400 MHz. The received response was then fed to the network analyzer. Fig. 4 (a) shows the measured 3-dB electrical modulation bandwidth of the UV-C $\mu$LED as a function of current density. As shown, the measured modulation bandwidth increases linearly with increasing current density from 18 to 71 A/cm$^2$, which is consistent with the relationship between the modulation bandwidth and current density we observed in our early work on visible $\mu$LEDs [12]. However, by further increasing the current density, the measured modulation bandwidth becomes saturated at around 438 MHz with a slight variation (less than 2 MHz). In order to explain this saturation, we compared the measured frequency responses of the $\mu$LED at different current densities. The typical frequency responses at 18 A/cm$^2$ (highlighted by the red circle in Fig. 4(a)) and 71 A/cm$^2$ (highlighted by the blue circle in Fig. 4(a)) are presented in Fig. 4(b) and (c), respectively. Compared with the frequency response at 18 A/cm$^2$, the one at 71 A/cm$^2$ shows a sharp drop when increasing the modulation frequency to around 450 MHz. It is noticed that the APD detector used for the measurement has the similar frequency response characteristic [23]. This indicates that the observed saturation of measured modulation bandwidth is actually caused by the APD rather than the $\mu$LED itself [24, 25]. Therefore, the modulation bandwidth of the $\mu$LED fabricated in this work is expected to be much higher than 438 MHz. We have tried to repeat the similar

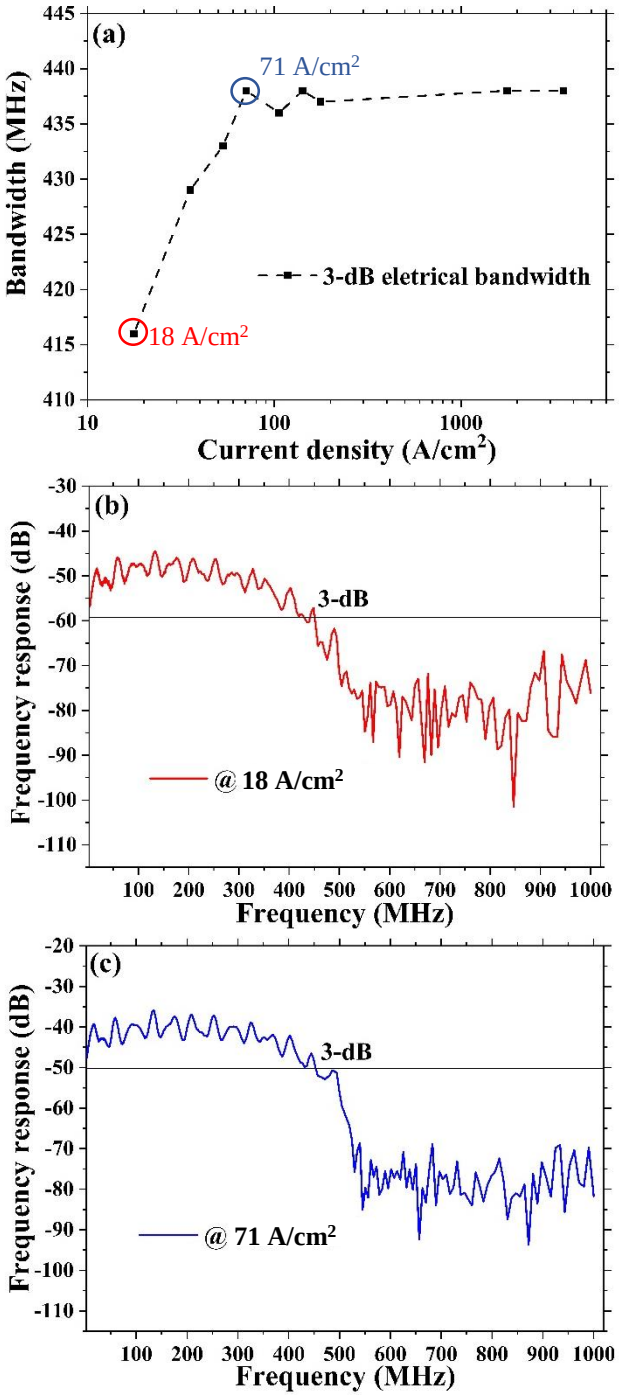


**Fig. 4.** (a) 3-dB electrical modulation bandwidth of the UV-C $\mu$LED as a function of current density; small signal frequency responses of the UV-C $\mu$LED at (b) 18 and (c) 71 A/cm$^2$.

measurements using a large bandwidth (2 GHz) deep UV PIN detector. However, due to the low sensitivity of the detector and low optical power of the UV-C $\mu$LED, no useful signal was detected. In order to overcome these issues, the performance of both APD and deep UV LEDs need to be further improved. Nevertheless, we emphasize that the UV-C $\mu$LED has a measured 3-dB electrical modulation bandwidth of 438 MHz at 71 A/cm$^2$. This value is already around 3 times higher than the reported 3-dB electrical modulation bandwidth of 153 MHz [3].

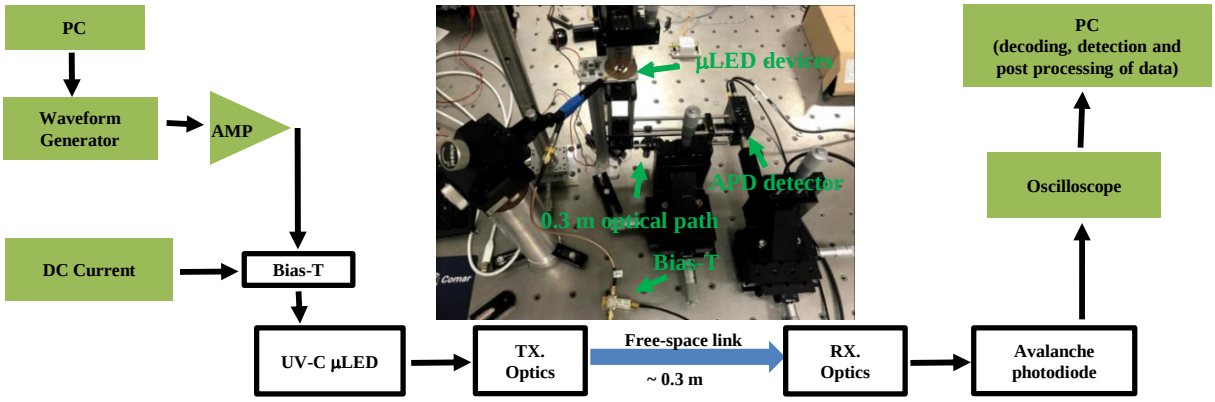


**Fig. 5.** Schematic diagram and optical image of experimental set up for the deep UV communication using the fabricated UV-C $\mu$LED.

Moreover, compared with our previous work based on visible c-plane $\mu$LEDs, this UV-C $\mu$LED also presents much larger modulation bandwidth even at low current densities. As mentioned above, the modulation bandwidth of $\mu$LEDs is dominated by their differential carrier lifetime which is the combination of radiative and non-radiative recombination lifetimes [13]. It is well known that the quality of the AlGaN-based deep UV LED wafer is relatively low due to the high-density defects generated in the material growth process [26]. This results in a shorter non-radiative recombination lifetime for UV-C $\mu$LEDs and, thus, large modulation bandwidth.

## 3. DEEP UV COMMUNICATIONS USING THE UV-C $\mu$LED LIGHT SOURCE

By using the fabricated UV-C $\mu$LED as a light source, a deep UV wireless communication system was implemented. In order to fully demonstrate the capability of this $\mu$LED for deep UV communications, single-carrier OOK and multi-carrier OFDM modulation schemes were both used in our experiments. Fig. 5 shows a schematic diagram and optical image of the setup used in this work. Both OOK and OFDM waveforms generated in MATLAB® were mapped to analog signals through an arbitrary waveform generator (AWG; Keysight 81180B). These analog signals from the AWG were then amplified by an amplifier (ZHL-6A-S+). Afterwards, the amplified analog signals and a DC bias current were combined by the bias-T and then applied to a UV-C $\mu$LED using a high speed micro-probe. In order to optimise the system performance, extensive tests were performed to determine the modulation signal depths ($V_{PP}$) and DC bias current densities ($J_{DC}$) used in the experiments. For the OOK modulation scheme, the $V_{PP}$ and $J_{DC}$ were set as 2 V and 1410 A/cm$^2$. For the OFDM modulation scheme, the $V_{PP}$ and $J_{DC}$ were set as 7 V and 1770 A/cm$^2$. The light emitted from the $\mu$LED was collected and focused into the UV enhanced Si APD detector by UV enhanced lens. The distance between the $\mu$LED and the APD detector was around 0.3 m. In this set up, a combination of light scattering and non-optimised collection optics and optical alignment results in only 20% of the emitted light power being received by the APD. It means around 26 and 30 $\mu$W optical power were illuminated onto the APD detector for OOK and OFDM modulation schemes, respectively. Improvement to this system is ongoing. The output signal of the APD detector was fed into a digital oscilloscope (Keysight, MSO7104B) and processed offline in MATLAB®.

### A. OOK modulation scheme

For the OOK modulation scheme, two information symbols were firstly mapped to different amplitudes and then further referred to as transmitted symbols. Non-return-to-zero (NRZ) symbols are used and the set of transmitted symbols are {-1, 1}. A root raised cosine filter was used before the transmitted symbols are sent to the AWG. To obtain the received symbol, the received signal was filtered by a matched filter and down-sampled. Fig. 6(a) illustrates the normalized number of occurrences of transmitted and received symbols of OOK represented by histograms at 800 Mbps. As shown, the distribution of symbols generated at the transmitter (black parts) is uniform but that of received symbols before the equalizer (blue parts) is negative-side heavier. This is mainly due to the so-called intersymbol interference (ISI) [27], which is caused by the amplitude and delay distortions from the communication channel. In order to mitigate this phenomenon, a feedforward equalizer based on the recursive least square updating algorithm was deployed. This equalizer estimates the received symbols which go beyond a decision threshold and, then, decodes them to their nearest transmitted symbols. As presented by the brown data in the Fig. 6(a), after the equalization, the spread of received symbols becomes narrow which leads to a lower BER. This reduces the decoding errors due to the ability to distinguish the correctly transmitted symbols at the receiver. Fig. 6(b) shows the eye diagram of the received signal assuming the OOK modulation scheme at 800 Mbps after equalization. As shown, the open eyes can be clearly distinguished demonstrating a communication link with a low BER. Higher data transmission rates cannot be measured due to the limitation from the bandwidth of the APD detector.

### B. OFDM modulation scheme

The influence of ISI on the BER in single carrier modulation scheme such as OOK would become more pronounced with the increase of the data transmission rate. As a result, the equalizer would be more computationally complex for high-speed communications [18]. A cost-effective way to simplify the equalizer is to apply OFDM with a single tap equalizer. The encoding method of the OFDM is done by modulating binary bits into $M$-ary quadrature amplitude modulation ($M$-QAM) symbols, where $M$ is the constellation order. Then, depending on the available SNR, different constellation sizes are loaded on the subcarriers using the adaptive bit and energy loading. An inverse fast Fourier transformation (IFFT) is used to multiplex

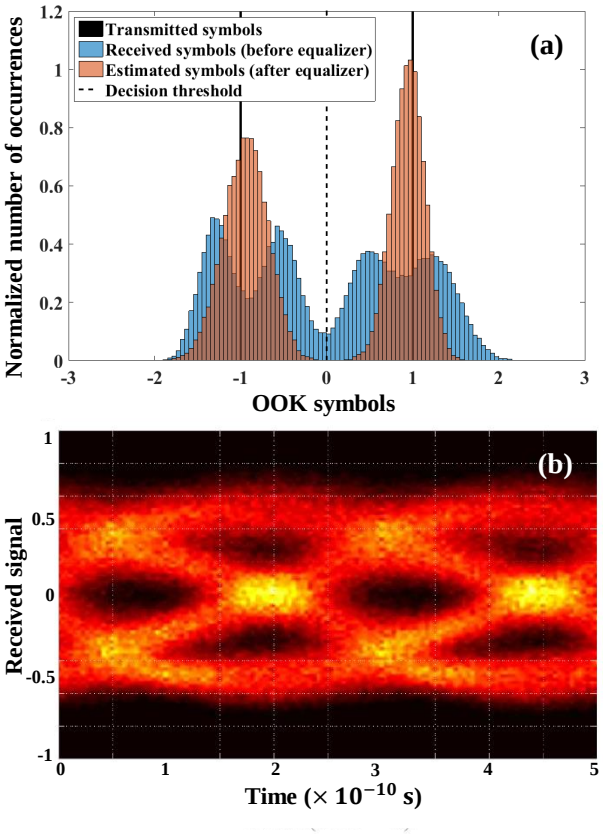


**Fig. 6.** (a) Normalized number of occurrences of transmitted and received symbols assuming the OOK modulation scheme at 800 Mbps and (b) the eye diagram of received symbols assuming the same measurement conditions using the UV-C $\mu$LED.

$N_{FFT}$/2-1 QAM symbols into $N_{FFT}$ subcarriers. By introducing Hermitian symmetry on the OFDM frame, a real-valued output is guaranteed. With the purpose of shifting the negative OFDM samples to positive, a DC bias is imposed. The details of this method could be found in our early work [18]. In this measurement, the sampling frequency of the AWG is 4 GS/s and the oversampling factor of the root raised cosine is set as 4. Fast Fourier transformation (FFT) is applied on the received signal and the received QAM symbols are equalized using the estimated channel. Fig. 7(a) shows the measured SNR versus bandwidth of UV-C $\mu$LED at $J_{DC}$ = 1770 A/cm$^2$ and $V_{PP}$ = 7 V and the recovered $M$-QAM constellations for $M$= 4, 8, 16 are inserted as well. The SNR performance of at least 5 dB is shown up to 480 MHz of bandwidth. This value is good enough for the decoder to distinguish the transmitted symbols from $M$-QAM constellations for $M$= 4, 8, 16, which enables high-speed deep UV communication. Fig. 7(b) presents the measured data transmission rates versus BER using the OFDM modulation scheme. Up to 1.1 Gbps data transmission rate is achieved at the BER of 3.8 $\times$ 10$^{-3}$. In Table 1, we compared our deep UV communication results with those from other published work. As listed, on the other hand, thanks to the high-bandwidth character of the used UV-C $\mu$LED, we achieved the highest data transmission rate at the BER of 3.8 $\times$ 10$^{-3}$ under the strong limitation from the APD detector used. Although the transmission distance of our work is strongly limited by the optical power produced from the UV-C $\mu$LED, this low optical power minimizes the adverse effects of UV radiation in communications.

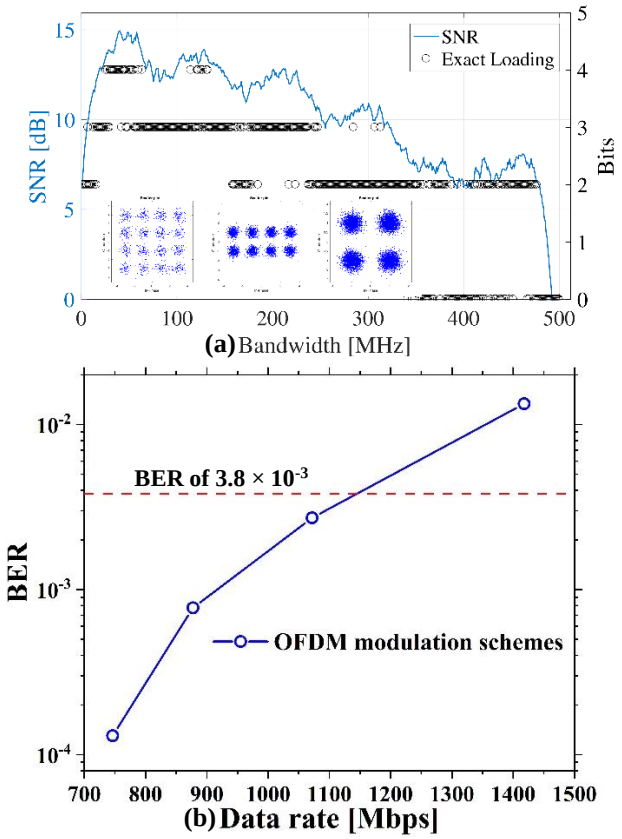


**Fig. 7.** (a) Measured SNR versus bandwidth for OFDM at $J_{DC}$= 1770 A/cm$^2$ and $V_{PP}$= 7 V. $M$-QAM constellation symbols received at the photodetector after equalization for $M$= 4, 8, 16 are inserted; (b) data transmission rate versus BER for OFDM measurement at $J_{DC}$= 1770 A/cm$^2$ and $V_{PP}$= 7 V.

## 4. CONCLUSION

The design, fabrication and performance of the III-nitride UV-C $\mu$LEDs are presented in this paper. Each UV-C $\mu$LED could be operated at a DC current density up to 3400 A/cm$^2$ with a directed optical power up to 196 $\mu$W. Due to the limitation of the commercial APD detector used in this work, the maximum measured 3-dB electrical modulation bandwidth of the UV-C $\mu$LED linearly increased in a small current density range, and saturated at 438 MHz at a current density of 71 A/cm$^2$. This modulation bandwidth is 3 times higher than the reported bandwidth of conventional deep UV LEDs. The UV-C $\mu$LED was further used as the light source in a free-space deep UV communication system. Thanks to its high-bandwidth character, up to 800 Mbps and 1.1 Gbps data transmission rates at BER of 3.8 $\times$ 10$^{-3}$ are achieved assuming OOK and OFDM modulation schemes, respectively. These high data transmission rates demonstrate the great potential of $\mu$LEDs for deep UV communications.

## ACKNOWLEDGMENTS

We acknowledge the "Qingdao Jason Electric Co., Ltd" for providing deep UV LED materials. This work was sup-

**Table 1. Comparison of deep UV communication results from the literature, compared to this work**

| Light source | Modulation Scheme | Transmission Power | Channel Length | Data Rate | BER | Ref |
|---|---|---|---|---|---|---|
| 265 nm mercury-xenon lamp | PPM | 25 W | 1.6 km | 1.2 Mbps | — | [8] |
| 253 nm mercury-argon lamp | PPM | 5 W | 0.5 km | 10 kbps | $10^{-5}$ | [9] |
| 254 nm low pressure mercury lamp | FSK | — | 6 m | 1.2 kbps | $10^{-4}$ | [6] |
| 265 nm LED arrays | OOK/PPM | 43 mW | 10 m | 2.4 kbps | $10^{-4}$ | [7] |
| 294 nm LED | OFDM | 190 $\mu$W | 0.08 m | 71 Mbps | $3.8 \times 10^{-3}$ | [10] |
| 280 nm LED | PAM-4 | — | 1.5 m | 1.6 Gbps | $2.0 \times 10^{-2}$ | [3] |
| 262 nm $\mu$LED | OFDM | 196 $\mu$W | 0.3 m | 1.1 Gbps | $3.8 \times 10^{-3}$ | This work |

ported by the Engineering and Physical Sciences Research Council (EPSRC) under grant EP/K00042X/1 "Ultra-parallel Visible Light Communications". The data is available online at https://doi.org/10.15129/0efd3fc2-7f3d-4647-bb56-8f470d80fed4.

## REFERENCES

1. M. S. Islim, S. Videv, M. Safari, E. Xie, J. J. D. McKendry, E. Gu, M. D. Dawson, and H. Haas, "The impact of solar irradiance on visible light communications," J. Light. Technol. (2018).
2. Z. Xu and B. M. Sadler, "Ultraviolet communications: potential and state-of-the-art," IEEE Commun. Mag. **46** (2008).
3. K. Kojima, Y. Yoshida, M. Shiraiwa, Y. Awaji, A. Kanno, N. Yamamoto, and S. Chichibu, "1.6-Gbps LED-Based Ultraviolet Communication at 280 nm in Direct Sunlight," in *2018 European Conference on Optical Communication (ECOC),* (IEEE, 2018), pp. 1–3.
4. S. Karp, R. M. Gagliardi, S. E. Moran, and L. B. Stotts, *Optical channels: fibers, clouds, water, and the atmosphere* (Springer Science & Business Media, 2013).
5. D. E. Sunstein, "A scatter communications link at ultraviolet frequencies." Ph.D. thesis, Massachusetts Institute of Technology (1968).
6. T. Feng, F. Xiong, Q. Ye, Z. Pan, Z. Dong, and Z. Fang, "Non-line-of-sight optical scattering communication based on solar-blind ultraviolet light," in *Optical Transmission, Switching, and Subsystems V,* , vol. 6783 (International Society for Optics and Photonics, 2007), p. 67833X.
7. D. Han, Y. Liu, K. Zhang, P. Luo, and M. Zhang, "Theoretical and experimental research on diversity reception technology in NLOS UV communication system," Opt. express **20**, 15833–15842 (2012).
8. J. J. Puschell and R. Bayse, "High data rate ultraviolet communication systems for the tactical battlefield," in *Tactical Communications Conference, 1990. Vol. 1. Tactical Communications. Challenges of the 1990's, Proceedings of the,* (IEEE, 1990), pp. 253–267.
9. M. Geller, T. E. Keenan, D. E. Altman, and R. H. Patterson, "Optical non-line-of-sight covert, secure high data communication system," (1985). US Patent 4,493,114.
10. X. Sun, Z. Zhang, A. Chaaban, T. K. Ng, C. Shen, R. Chen, J. Yan, H. Sun, X. Li, J. Wang *et al.*, "71-Mbit/s ultraviolet-B LED communication link based on 8-QAM-OFDM modulation," Opt. express **25**, 23267–23274 (2017).
11. E. Xie, M. Stonehouse, R. Ferreira, J. J. McKendry, J. Herrnsdorf, X. He, S. Rajbhandari, H. Chun, A. V. Jalajakumari, O. Almer *et al.*, "Design, Fabrication, and Application of GaN-Based Micro-LED Arrays With Individual Addressing by N-Electrodes," IEEE Photonics J. **9**, 1–11 (2017).
12. S. Rajbhandari, J. J. McKendry, J. Herrnsdorf, H. Chun, G. Faulkner, H. Haas, I. M. Watson, D. O'Brien, and M. D. Dawson, "A review of gallium nitride LEDs for multi-gigabit-per-second visible light data communications," Semicond. Sci. Technol. **32**, 023001 (2017).
13. E. F. Schubert, *Light-emitting diodes* (E. Fred Schubert, 2018).
14. J. J. McKendry, R. P. Green, A. Kelly, Z. Gong, B. Guilhabert, D. Massoubre, E. Gu, and M. D. Dawson, "High-speed visible light communications using individual pixels in a micro light-emitting diode array," IEEE Photonics Technol. Lett. **22**, 1346–1348 (2010).
15. R. X. Ferreira, E. Xie, J. J. McKendry, S. Rajbhandari, H. Chun, G. Faulkner, S. Watson, A. E. Kelly, E. Gu, R. V. Penty *et al.*, "High bandwidth GaN-based micro-LEDs for multi-Gb/s visible light communications," IEEE Photonics Technol. Lett. **28**, 2023–2026 (2016).
16. A. Rashidi, M. Monavarian, A. Aragon, A. Rishinaramangalam, and D. Feezell, "GHz-Bandwidth Nonpolar InGaN/GaN Micro-LED Operating at Low Current Density for Visible-Light Communication," in *2018 IEEE International Semiconductor Laser Conference (ISLC),* (IEEE, 2018), pp. 1–2.
17. A. Rashidi, M. Monavarian, A. Aragon, A. Rishinaramangalam, and D. Feezell, "Nonpolar $m$ -Plane InGaN/GaN Micro-Scale Light-Emitting Diode With 1.5 GHz Modulation Bandwidth," IEEE Electron Device Lett. **39**, 520–523 (2018).
18. M. S. Islim, R. X. Ferreira, X. He, E. Xie, S. Videv, S. Viola, S. Watson, N. Bamiedakis, R. V. Penty, I. H. White *et al.*, "Towards 10 Gb/s orthogonal frequency division multiplexing-based visible light communication using a GaN violet micro-LED," Photonics Res. **5**, A35–A43 (2017).
19. J. J. McKendry, D. Tsonev, R. Ferreira, S. Videv, A. D. Griffiths, S. Watson, E. Gu, A. E. Kelly, H. Haas, and M. D. Dawson, "Gb/s single-LED OFDM-based VLC using violet and UV gallium nitride $\mu$LEDs," in *Summer Topicals Meeting Series (SUM), 2015,* (IEEE, 2015), pp. 175–176.
20. N. Maeda, M. Jo, and H. Hirayama, "Improving the Efficiency of AlGaN Deep-UV LEDs by Using Highly Reflective Ni/Al p-Type Electrodes," physica status solidi (a) **215**, 1700435 (2018).
21. M. Kneissl, "A brief review of III-nitride UV emitter technologies and their applications," in *III-nitride ultraviolet emitters,* (Springer, 2016), pp. 1–25.
22. G.-D. Hao, M. Taniguchi, N. Tamari, and S.-i. Inoue, "Enhanced wall-plug efficiency in AlGaN-based deep-ultraviolet light-emitting diodes with uniform current spreading p-electrode structures," J. Phys. D: Appl. Phys. **49**, 235101 (2016).
23. Thorlabs, "APD 430x operation Manual," http://www.thorlabs.com/drawings/90bcb90dcbbce65d-E6B5D51A-F5C5-66C3-DE56D698D3E3D2D6/APD430A2_M-Manual.pdf.
24. R. P. Green, J. J. McKendry, D. Massoubre, E. Gu, M. D. Dawson, and A. E. Kelly, "Modulation bandwidth studies of recombination processes in blue and green InGaN quantum well micro-light-emitting diodes,"

Appl. Phys. Lett. **102**, 091103 (2013).
25. J. Cho, E. Yoon, Y. Park, W. J. Ha, and J. K. Kim, "Characteristics of blue and ultraviolet light-emitting diodes with current density and temperature," Electron. Mater. Lett. **6**, 51–53 (2010).
26. M. Shatalov, W. Sun, A. Lunev, X. Hu, A. Dobrinsky, Y. Bilenko, J. Yang, M. Shur, R. Gaska, C. Moe *et al.*, "Algan deep-ultraviolet light-emitting diodes with external quantum efficiency above 10%," Appl. Phys. Express **5**, 082101 (2012).
27. J. G. Proakis, "Digital communications. 1995," McGraw-Hill, New York .